Path Loss Modeling in Urban Water–Land Environments at 28 GHz: Considering Water Surface Reflection and Building Diffraction

Xi Liao, *Senior Member, IEEE*, Xuan Li, Yang Wang, *Senior Member, IEEE*, Jihua Zhou, Tao Zhao, and Jie Zhang, *Senior Member, IEEE*

***Abstract*—This letter proposes a path loss model in urban water–land environments for line-of-sight (LOS) and non-LOS (NLOS) propagation at millimeter-wave (mm-wave) band, in which water surface reflection and building diffraction are considered simultaneously. An extensive measurement campaign in a campus pond environment at 28 GHz is conducted. Other channel characteristics, such as power delay profile and root-mean-square delay spread are also analyzed. Results indicate that the proposed model can predict the path loss in urban water–land environments accurately. This work can be applied to the deployment of wireless networks in urban water–land environments.**

***Index Terms*—Channel measurement, millimeter wave, path loss, radio propagation.**

I. Introduction

SMART water affair is an important part of smart city construction. In order to achieve seamless full coverage and provide ultra-high-speed and extremely low-delay networks in the city [1], it is essential to deploy the millimeter-wave (mm-wave) communication in the urban water–land environments. Since the propagation mechanism becomes more complex in urban water–land environments, it requires a good understanding of the propagation characteristics, such as path loss, power delay profile, and root-mean-square (rms) delay spread. However, radio propagation in urban water–land environments at the mm-wave band have not been thoroughly investigated compared to in other environments, such as the open sea and rain forest [2].

Looking from the existing literature on water environments, International Telecommunication Union (ITU) P.1546 suggested an empirical path loss model in the marine environment from 30 to 3000 MHz [3], it was a function of distance, antenna height, frequency, and percentage of time. Furthermore, the floating intercept (FI) model and close-in reference distance (CI) model have been used to predict path loss in the maritime environment at the mm-wave band [4], [5]; they described the influence of the distance and shadow fading. Also, the two-ray model has been widely adopted to investigate the effect of water surface reflection on path loss [6], [7]. However, the majority of these works assumed a smooth water surface [8]. A modified two-ray model introduced a coefficient in the power of exponential function to predict the behavior of maritime channels better at 35 and 94 GHz [9]. However, the modified two-ray model can only be applicable in situations with wide ocean surface environments. A new model based on geometrical optics and the uniform theory of diffraction (UTD) was proposed to calculate propagation loss in dense forests and river environments [10]. ITU-R P.1411 [11] has classified the microcell more specifically as a picocell, which was suitable for mm-wave short-range communication. To the best of our knowledge, the urban water–land picocell environment at mm-wave has not been fully investigated.

The aim of this letter is encouraged by the need to provide an accurate path loss model in urban water–land scenarios at mm-wave bands. An experimental platform is set up to validate the accuracy of the proposed model. Contributions of this letter are summarized as follows.

1) Based on the theory of radio propagation and geometric channel modeling [12], [13], [14], we propose a path loss model in the urban water–land environment for line-of-sight (LOS) and non-LOS (NLOS) propagation at the mm-wave band. For LOS propagation, on one hand, the proposed model modifies the reflection coefficient in the two-ray model based on the single Debye relaxation model, and on the other hand, the proposed model simplifies the diffraction coefficient in the UTD model by

Manuscript received 27 October 2022; accepted 16 November 2022. Date of publication 23 November 2022; date of current version 7 April 2023. This work was supported in part by the National Natural Science Foundation of China under Grant 62271095 and Grant 62171071; and in part by the Natural Science Foundation of Chongqing under Grant cstc2021jcyj-msxmX0634. *(Corresponding author: Yang Wang.)*

Xi Liao, Xuan Li, and Yang Wang are with the School of Communication and Information Engineering, Chongqing University of Posts and Telecommunications, Chongqing 400065, China, and also with the Chongqing Key Laboratory of Complex Environmental Communications, Chongqing 400065, China (e-mail: liaoxi@cqupt.edu.cn; s200131096@edu.cqupt.edu.cn; wangyang@cqupt.edu.cn).

Jihua Zhou and Tao Zhao are with the Aerospace New Generation Communications Co., Ltd, Chongqing 401332, China (e-mail: jhzhou@ict.ac.cn; zwindt@126.com).

Jie Zhang is with the Department of Electronic and Electrical Engineering, University of Sheffield, S10 2TN Sheffield, U.K. (e-mail: zhangjie123@cqupt.edu.cn).

Digital Object Identifier 10.1109/LAWP.2022.3224155

classifying different types of obstacles. For NLOS propagation, the proposed model consists of the reflection loss, diffraction loss, and a frequency-dependent correction factor.

2) We conduct channel measurement campaigns in campus pond environments at 28 GHz. Six receiver (Rx) positions in the LOS case and four Rx positions in the NLOS case are measured. The main channel characteristics, including path loss, power delay profile, and rms delay spread, are analyzed.

The rest of this letter is organized as follows. Section II proposes a path loss model in the urban water environment for LOS and NLOS propagation conditions at the mm-wave band. Section III introduces the measurement setup and the measurement deployment. Section IV presents the results of the measured value, evaluates the accuracy of the proposed model, and analyzes channel characteristics. Finally, conclusions are summarized in Section V.

II. Path Loss Modeling

A. Path Loss Modeling for LOS Propagation

For LOS propagation, we assume that there exists the direct path, reflected path, and diffracted path, so the path loss $L_{\text{LOS}}(f)$ can be expressed as

$$L_{\text{LOS}}(f) = L_{2-\text{ray}} + L_{\text{diff}} - L(f) \tag{1}$$

where $L_{2-\text{ray}}$ denotes the path loss caused by the directed path and the reflected path from the water surface. Moreover, L_{diff} is the diffraction loss caused by obstacles.

In order to take the effect of frequency changes on path loss into account, a frequency-dependent value $L(f)$ is introduced, and it can be calculated in decibels as [15]

$$L(f) = n_o \cdot 10\log_{10}\frac{f}{f_0} \tag{2}$$

where f_0 is the reference frequency, $n_0 = \log_e |f - f_0|$ denotes the frequency index.

The majority of existing works have been based on the assumption that the water surface was smooth and the reflection coefficient was -1. However, the roughness of the water surface cannot be ignored at the mm-wave band according to the Rayleigh criterion [16]. So the scattering loss factor ρ_s can be calculated as [17]

$$\rho_s = \exp\left[-8\left(\frac{\pi\sigma_h\cos\theta}{\lambda}\right)^2\right] \tag{3}$$

where σ_h is the standard deviation of the water surface height relative to the average surface height, θ indicates the angle of incidence, and λ is the wavelength. Thus, the reflection coefficient R_{rough} is calculated as

$$R_{\text{rough}} = \rho_s R \tag{4}$$

where R represents the dielectric reflection coefficient, which is in relation to the dielectric constant ε.

Note that the complex permittivity of water is greatly affected by frequency, so it cannot be replaced by a fixed value in traditional methods [18]. So we introduced the single Debye relaxation model, the dielectric constant ε can be given by [19]

$$\varepsilon = \left|\varepsilon_0 - \frac{(\varepsilon_0 - 5.48)\, f}{f - j f_p}\right| \tag{5}$$

where

$$\begin{aligned} \varepsilon_0 &= 77.66 + 103.3 \cdot \theta_T \\ f_p &= 20.09 - 142 \cdot \theta_T + 294 \cdot \theta_T^2 \\ \theta_T &= \frac{300}{273.15 + T} - 1 \end{aligned} \tag{6}$$

where T denotes the temperature in °C.

The total E-field can be given by $\boldsymbol{E}_{2-\text{ray}} = \boldsymbol{E}_{\text{LOS}} + \boldsymbol{E}_{\text{Ref}}$, where E_{LOS} and E_{Ref} are the E-field due to the directed path and the reflected path, respectively [14]. As a result, the received power P_r can be calculated as [20]

$$\begin{aligned} P_r &= \frac{|\boldsymbol{E}_{2-\text{ray}}|^2}{2\eta_0} \\ &= P_t G_t G_r \left(\frac{1}{4\pi d/\lambda}\right)^2 \left|1 + R_{\text{rough}} \cdot e^{j\Delta\Phi}\right|^2 \end{aligned} \tag{7}$$

where η_0 indicates the intrinsic impedance of free space, P_t, G_t, and G_r are the transmitted power, the antenna gain of transmitter (Tx) and Rx, respectively. Moreover, $\Delta\Phi$ is a phase difference that can be expressed as $\Delta\Phi = \frac{4\pi h_t h_r}{\lambda d}$, d stands for the distance between the transmitter and receiver, h_t and h_r are the height of Tx and Rx, respectively. Thus, the path loss $L_{2-\text{ray}}$ can be written as

$$L_{2-\text{ray}} = 20\log_{10}\left(\frac{\lambda}{4\pi d}\left(1 + R_{\text{rough}} \cdot e^{j\Delta\Phi}\right)\right). \tag{8}$$

To study the path loss caused by diffraction propagation, we select the UTD method to compute diffraction loss for LOS and NLOS propagation in this letter. The subroutines produced by the UTD are only slightly more computationally intensive than those for knife-edge diffraction but can account for surface roughness and electrical properties of the building material [21]. According to the work in [22], we classified the diffraction objects as regular right-angle wedges or other regular shapes, the diffraction loss L_{Diff} can be given as

$$L_{\text{Diff}} = \left(\frac{4\pi}{\lambda}\right)^2 \frac{\cos^2\Psi}{D^2_{\text{right-angle}}} x_1 x_2 (x_1 + x_2) \tag{9}$$

where Ψ refers to the viewing angle from the Tx antenna to the Rx antenna, which is dependent on the height of the antennas, $D_{\text{right-angle}}$ represents the diffraction coefficient at the objects with right-angle wedges or other regular shapes, and x_1, x_2 are the distances from the diffraction point to the Tx and Rx, respectively.

B. Path Loss Modeling for NLOS Propagation

For NLOS propagation, we assume that the path loss is determined by the reflection loss and diffraction loss, so the path loss $L_{\text{NLOS}}(f)$ can be calculated as

$$L_{\text{NLOS}}(f) = L_{Ref} + L_{\text{diff}} - L(f) \tag{10}$$

(a)

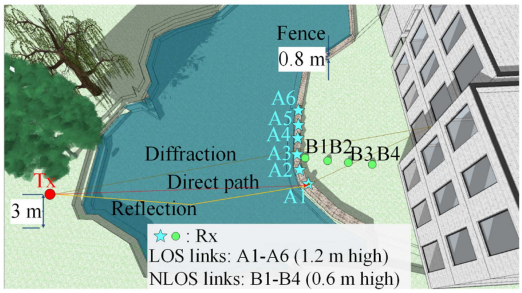

(b)

Fig. 1. Layout of the measurement campaign. (a) Campus pond environment. (b) Layout of the pond.

where L_{Ref} stands for the path loss caused by the reflected path. By calculating field strength E_{Ref}, the reflection loss model can be expressed as

$$L_{\text{Ref}} = 20\log_{10}\left(\frac{\lambda}{4\pi d}\right) + 10\log_{10}\left(R_{\text{rough}} \cdot e^{j\Delta\Phi}\left(2 + R_{\text{rough}} \cdot e^{j\Delta\Phi}\right)\right). \tag{11}$$

III. Measurement Campaign

The structure of the measurement system is shown in Fig. 1, consisting of a vector network analyzer (VNA), a low-noise amplifier (LNA), and Tx and Rx modules. The Tx and Rx modules are mounted on mechanical parts, which include a rotator, a tripod, and a cart. In order to scan the spatial domain and capture multipath components (MPCs) from various directions, the rotator is used to mechanically rotate Rx in both the azimuth plane and the elevation plane. The LNA is used to reduce noise interference. The transceivers are connected to the ports of the VNA via cables, and a laptop is used to control the rotators as well as to record data from the VNA.

This measurement is conducted at a center frequency of 28 GHz with 2 GHz bandwidth and 1001 frequency points, and the delay resolution is 0.5 ns. The VNA intermediate frequency (IF) bandwidth is set to 1 kHz to reduce the impact of noise. The Tx is equipped with an omnidirectional antenna with 4.2 dBi gain and the height of 3 m from the ground. The Rx is equipped with a horn antenna with 20.6 dBi gain and 15.6° half-power beamwidth (HPBW). The heights of the Rx are 0.6 m and 1.2 m from the ground, respectively. Rx scans the spatial domain with a 10° angle resolution, from 0° to 360° in the azimuth plane, and from −20° to 20° in the elevation plane. The detailed system parameters are listed in Table I.

TABLE I
Measurement Parameters

Parameters	Symbols	Value
Center frequency	f	28 GHz
Bandwidth	B	2 GHz
IF bandwidth	–	1 kHz
Frequency resolution	–	2 MHz
Sweeping points	–	1001
Transmitted power	P_t	0 dBm
Tx antenna	–	Omnidirectional antenna
Rx antenna	–	Horn antennas
Tx height	h_t	3 m
Rx height	h_r	1.2 m/0.6 m
Antenna gain of Tx	G_t	4.2 dBi
Antenna gain of Rx	G_r	20.6 dBi
LOS links	–	A1-A6
NLOS links	–	B1-B4
HPBW of Rx antenna	–	15.6°
Rx azimuth rotation range	–	[0°, 360°]
Rx azimuth rotation step	–	10°
Rx elevation rotation range	–	[-20°, 20°]
Rx elevation rotation step	–	10°
Gain of LNA	G	35 dB

The measurement campaign is conducted in a pond of Chongqing University of Posts and Telecommunications, as shown in Fig. 1(a). The pond is a wide water–land environment and there are buildings distributed on one side and a concrete fence with a height of 0.8 m surrounds the pond. So it is possible to carry out both LOS and NLOS measurements by adjusting the height of Rx. The positions of the Tx and Rx are shown in Fig. 1(b). Tx is located at a fixed position, and overall 10 Rx positions are selected. A1–A6 are deployed on the fence as the LOS links. Moreover, B1–B4 are placed behind the fence and make up the NLOS links. They are uniformly distributed with a 2 m distance interval.

IV. Results Analysis

A. Power Delay Profile

PDP reveals the power strength of the received signal and the travel time of the arrived resolvable MPCs. Based on the data processing, PDP is defined as

$$P(\tau_l) = |h(\tau_l)|^2 \tag{12}$$

where $h(\tau_l)$ refers to the value of the channel impulse responses in the τ_lth delay, and τ_l represents the excess delay of the lth component.

Fig. 2 shows PDPs in LOS and NLOS scenarios at A3 and B1. For the LOS condition at A3, the mean value of the noise power is −57 dB, and a LOS component can be clearly observed with received power about −35.12 dB and delay of 14.76 ns. Furthermore, other reflection and diffraction components caused by the water surface and buildings can be seen with the power degradation of 10–20 dB compared with the LOS component. For the NLOS condition at B1, MPCs can also be clearly identified. However, the NLOS power is significantly lower than that of LOS since the fence blocking between Tx and Rx.

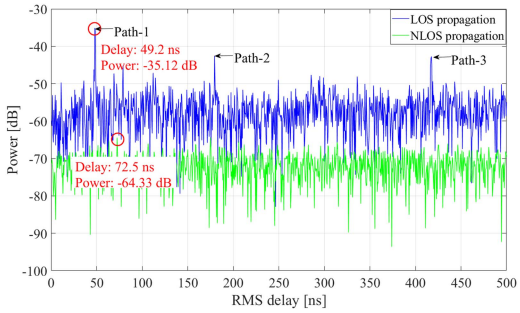

Fig. 2. Power delay profile under LOS and NLOS conditions.

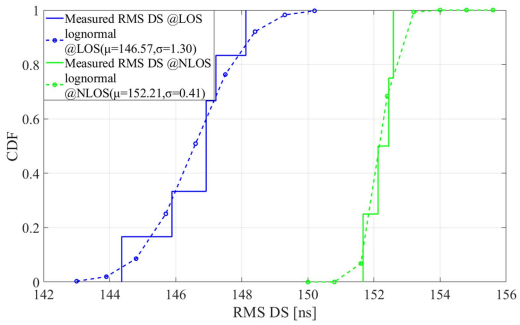

Fig. 3. CDF of rms delay spread under LOS and NLOS conditions.

B. RMS Delay Spread

The time dispersion properties of wideband channels are generally characterized by rms DS, it is defined as the square root of the second central moment of the PDP [23]. Fig. 3. plots the log-normal fitting to the cumulative distribution functions (cdf) of rms DS in LOS and NLOS scenarios. The cdfs of lognormal distributions fit well with the measured data, and the mean values of rms DS are 146.57 ns and 152.21 ns in LOS and NLOS scenarios, respectively. The NLOS locations are found to have greater rms DS than LOS locations, since obstructions in NLOS locations block the direct path, causing MPCs to arrive at the receiver over a larger propagation time interval.

C. Path Loss

Fig. 4 illustrates the comparison of path loss scatter plots with the proposed model, CI model [4], FI model [5], two-ray model [6], reflection loss model [6], and ITU-R P.1411 model [11] under LOS and NLOS propagation conditions at 28 GHz. The proposed model fits well with the measured path loss model. For the CI model, the path loss exponent (PLE) n is 1.94, which is less than the theoretical free space PLE of 2. The PLE grows to 2.41 in the NLOS environment, indicating that the water–land mm-wave propagation channel experiences constructive interference from water surface reflections and obstacle diffractions. Moreover, the FI model and ITU-R P.1411 model have similar performance to the CI model. However, the errors of the two-ray model and reflection loss model are greater than 20 dB with measured path loss.

In addition, Table II shows the rms error [24] of the above path loss models with the measured path loss. In the LOS condition, the FI model has the minimum value of 0.64 dB. However, the proposed model is just 0.04 dB greater than that of the FI model under the LOS condition while the proposed model has the lowest value of 1.15 dB under the NLOS condition. It suggests that the proposed model has the best performance compared with other models; it can predict oscillations caused by the destructive combination of water surface reflection and building diffraction more accurately.

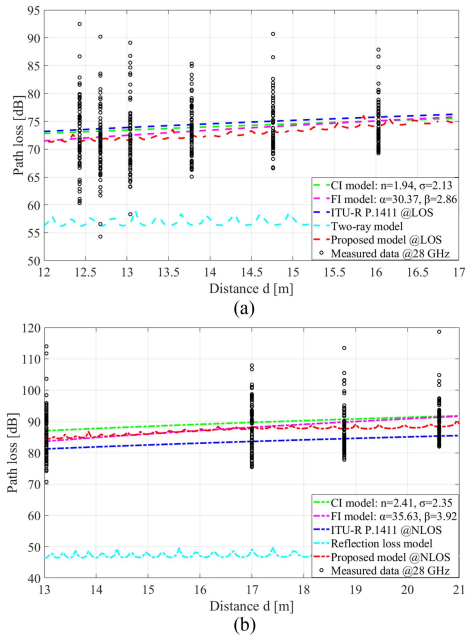

Fig. 4. Comparison of different path loss models under LOS and NLOS propagation conditions. (a) LOS propagation. (b) NLOS propagation.

TABLE II
RMSE OF DIFFERENT MODELS

Models	LOS	NLOS
CI model	1.15 dB	2.5 dB
FI model	0.64 dB	2.24 dB
ITU-R P.1411	1.59 dB	4.01 dB
Two-ray model	16.18 dB	-
Reflection loss model	-	39.80 dB
Proposed model	0.69 dB	1.15 dB

V. CONCLUSION

In this letter, we propose a path loss model that describes the water surface reflection loss and obstacle diffraction loss and introduces a frequency-dependent correction factor in the urban water–land environment at the mm-wave band. Based on an extensive measurement campaign in a pond scenario, the propagation characteristics including PDP, rms DS, and path loss are analyzed. It is found that there are a number of reflection and diffraction components in the water–land environment. Furthermore, the proposed model exhibits the best performance than other theoretical path loss models. The further analysis of channel modeling in the urban water–land environment will be presented in the future work.

REFERENCES

[1] S. A. Busari, S. Mumtaz, S. Al-Rubaye, and J. Rodriguez, "5G millimeter-wave mobile broadband: Performance and challenges," *IEEE Commun. Mag.*, vol. 56, no. 6, pp. 137–143, Jun. 2018.

[2] A. Danklmayer, G. Biegel, T. Brehm, S. Sieger, and J. Förster, "Millimeter wave propagation above the sea surface during the Squirrel campaign," in *Proc. 16th Int. Radar Symp.*, 2015, pp. 300–304.

[3] Method for Point-to Area Predictions for Terrestrial Services in the Frequency Range 30 MHz to 3000 MHz, Rec. ITU-R P.1546-5, International Telecommunications Union, Geneva, Switzerland, Sep. 2013.

[4] S. Sun et al., "Investigation of prediction accuracy, sensitivity, and parameter stability of large-scale propagation path loss models for 5G wireless communications," *IEEE Trans. Veh. Technol.*, vol. 65, no. 5, pp. 2843–2860, May 2016.

[5] S. Sun, T. S. Rappaport, M. Shafi, P. Tang, J. Zhang, and P. J. Smith, "Propagation models and performance evaluation for 5G millimeter-wave bands," *IEEE Trans. Veh. Technol.*, vol. 67, no. 9, pp. 8422–8439, Sep. 2018.

[6] Y. Lee, F. Dong, and Y. Meng, "Near sea-surface mobile radiowave propagation at 5 GHz: Measurements and modeling," *Radioengineering*, vol. 23, no. 3, pp. 824–830, 2014.

[7] J. Lee, J. Choi, W. Lee, J. Choi, and S. Kim, "Measurement and analysis on land-to-ship offshore wireless channel in 2.4 GHz," *IEEE Wireless Commun. Lett.*, vol. 6, no. 2, pp. 222–225, Apr. 2017.

[8] M. G. Gaitan, P. M. Santos, L. Pinto, and L. Almeida, "Experimental evaluation of the two-ray model for near-shore WiFi-based network systems design," in *Proc. IEEE 91st Veh. Technol. Conf.*, 2020, pp. 1–3.

[9] N. Mehrnia and M. K. Ozdemir, "Novel maritime channel models for millimeter radiowaves," in *Proc. 24th Int. Conf. Softw., Telecommun. Comput. Netw.*, 2016, pp. 1–6.

[10] L. E. C. Eras, D. K. N. da Silva, L. Correia, F. J. B. Barros, J. P. L. de Araujo, and G. P. dos S. Cavalcante, "A radio propagation model for a rainforest–river environment using UTD and geometrical optics," *IEEE Antennas Wireless Propag. Lett.*, vol. 21, no. 1, pp. 54–58, Jan. 2022.

[11] Propagation Data and Prediction Methods for the Planning of Short-Range Outdoor Radiocommunication Systems and Radio Local Area Networks in the Frequency Range 300 MHz to 100 GHz, Recommendation ITU-R P.1411-11, International Telecommunications Union, Geneva, Switzerland, Oct. 2021.

[12] R. He, B. Ai, G. L. Stüber, G. Wang, and Z. Zhong, "Geometrical-based modeling for millimeter-wave MIMO mobile-to-mobile channels," *IEEE Trans. Veh. Technol.*, vol. 67, no. 4, pp. 2848–2863, Apr. 2018.

[13] L. Tian, V. Degli-Esposti, E. M. Vitucci, and X. Yin, "Semi-deterministic radio channel modeling based on graph theory and ray-tracing," *IEEE Trans. Antennas Propag.*, vol. 64, no. 6, pp. 2475–2486, Jun. 2016.

[14] W. Wang, T. Jost, and R. Raulefs, "A semi-deterministic path loss model for in-harbor LoS and NLoS environment," *IEEE Trans. Antennas Propag.*, vol. 65, no. 12, pp. 7399–7404, Dec. 2017.

[15] W. C. Y. Lee, *Mobile Cellular Telecommunications*. New York, NY, USA: McGraw-Hill, 1995.

[16] P. Xie, K. Guan, D. He, H. Yi, J. Dou, and Z. Zhong, "Terahertz wave propagation characteristics on rough surfaces based on full-wave simulations," *Radio Sci.*, vol. 57, no. 6, 2022, Art. no. e2021RS007385.

[17] L. Xing, Y. Huang, Q. Xu, S. Alja'afreh, and T. Liu, "Complex permittivity of water-based liquids for liquid antennas," *IEEE Antennas Wireless Propag. Lett.*, vol. 15, pp. 1626–1629, 2016.

[18] T. S. Rappaport, *Wireless Communications: Principles and Practice*. Englewood Cliffs, NJ, USA: Prentice-Hall, 1996.

[19] T. Manabe, H. J. Liebe, and G. A. Hufford, "Complex permittivity of water between 0 and 30th," in *Proc. 12th Int. Conf. Infrared Millimeter Waves*, 1987, pp. 229–230.

[20] D. Couillard, G. Dahman, M. E. Grandmaison, G. Poitau, and F. Gagnon, "Robust broadband maritime communications: Theoretical and experimental validation," *Radio Sci.*, vol. 53, no. 6, pp. 749–760, 2018.

[21] J. D. Parsons, *The Mobile Radio Propagation Channel*. 2nd ed. Chichester, U.K.: Wiley, 2000.

[22] H. L. Bertoni, *Radio Propagation for Modern Wireless Systems*. Upper Saddle River, NJ, USA: Prentice-Hall, 2000.

[23] Y. Zahedi, R. Ngah, U. A. K. Chude-Okonkwo, S. Nunoo, and M. Mokayef, "Modeling the RMS delay spread in time-varying UWB communication channels," in *Proc. 5th Int. Conf. Intell. Adv. Syst.*, 2014, pp. 1–5.

[24] S. K. Hinga and A. A. Atayero, "Deterministic 5G mm-Wave large-scale 3D path loss model for Lagos Island, Nigeria," *IEEE Access*, vol. 9, pp. 134270–134288, 2021.